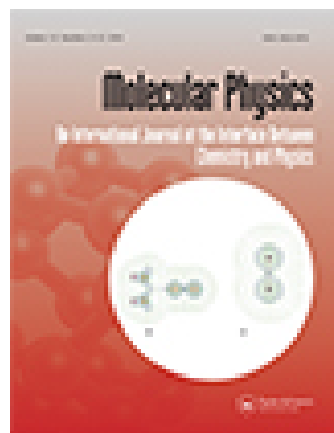


This article was downloaded by: [Florida Institute of Technology]

On: 19 March 2015, At: 05:33

Publisher: Taylor & Francis

Informa Ltd Registered in England and Wales Registered Number: 1072954 Registered office: Mortimer House, 37-41 Mortimer Street, London W1T 3JH, UK



[Click for updates](#)

Molecular Physics: An International Journal at the Interface Between Chemistry and Physics

Publication details, including instructions for authors and subscription information:

<http://www.tandfonline.com/loi/tmph20>

The dominance of small ions in the electric double layer of size- and charge-asymmetric electrolytes: a mean-field study on the charge reversal and surface charge amplification

Evelyn Angélica Barrios-Contreras^a, Enrique González-Tovar^a & Guillermo Iván Guerrero-García^{ab}

^a Instituto de Física, Universidad Autónoma de San Luis Potosí, San Luis Potosí, Mexico

^b Department of Materials Science and Engineering, Northwestern University, Evanston, IL, USA

Published online: 13 Mar 2015.

To cite this article: Evelyn Angélica Barrios-Contreras, Enrique González-Tovar & Guillermo Iván Guerrero-García (2015): The dominance of small ions in the electric double layer of size- and charge-asymmetric electrolytes: a mean-field study on the charge reversal and surface charge amplification, *Molecular Physics: An International Journal at the Interface Between Chemistry and Physics*, DOI: [10.1080/00268976.2015.1018853](https://doi.org/10.1080/00268976.2015.1018853)

To link to this article: <http://dx.doi.org/10.1080/00268976.2015.1018853>

PLEASE SCROLL DOWN FOR ARTICLE

Taylor & Francis makes every effort to ensure the accuracy of all the information (the "Content") contained in the publications on our platform. However, Taylor & Francis, our agents, and our licensors make no representations or warranties whatsoever as to the accuracy, completeness, or suitability for any purpose of the Content. Any opinions and views expressed in this publication are the opinions and views of the authors, and are not the views of or endorsed by Taylor & Francis. The accuracy of the Content should not be relied upon and should be independently verified with primary sources of information. Taylor and Francis shall not be liable for any losses, actions, claims, proceedings, demands, costs, expenses, damages, and other liabilities whatsoever or howsoever caused arising directly or indirectly in connection with, in relation to or arising out of the use of the Content.

This article may be used for research, teaching, and private study purposes. Any substantial or systematic reproduction, redistribution, reselling, loan, sub-licensing, systematic supply, or distribution in any form to anyone is expressly forbidden. Terms & Conditions of access and use can be found at <http://www.tandfonline.com/page/terms-and-conditions>

SPECIAL ISSUE IN HONOUR OF TOMAS BOUBLIK, IVO NEZBEDA, THE CZECH SCHOOL OF STATISTICAL MECHANICS AND THE LIBLICE CONFERENCE

The dominance of small ions in the electric double layer of size- and charge-asymmetric electrolytes: a mean-field study on the charge reversal and surface charge amplification

Evelyn Angélica Barrios-Contreras^a, Enrique González-Tovar^a and Guillermo Iván Guerrero-García  ^{a,b,*}

^aInstituto de Física, Universidad Autónoma de San Luis Potosí, San Luis Potosí, Mexico; ^bDepartment of Materials Science and Engineering, Northwestern University, Evanston, IL, USA

(Received 15 November 2014; accepted 9 February 2015)

The dominance of counterions in the electric double layer of size-asymmetric semi-punctual ions was proposed more than 30 years ago by Valleau and Torrie. According to their theoretical prescription, at large colloidal surface charges, the double layer properties of a fully asymmetric binary electrolyte become similar to those of a completely symmetric electrolyte if the properties of counterions are the same in both instances. In the same theoretical framework, we propose here that, for a fixed concentration of the smallest ionic species and weakly/moderate colloidal surface charges, the valence of small ions rules or mainly determines the structural and thermodynamic properties of the electric double layer regardless of the colloidal polarity. In other words, we show that the characteristics of the small ions dominate the double layer structure of non-highly charged colloids, independently if the small ions are coions or counterions. This is illustrated by a comprehensive analysis of the ionic and integrated charge profiles around a spherical macroion immersed in a fully size- and charge-asymmetric semi-punctual electrolyte. Charge reversal and surface charge amplification are observed in the regime of low/medium colloidal surface charge densities. The origin of these counterintuitive phenomena, and their corresponding *localisation* properties in the Helmholtz zone, are explained in terms of the electric double layer structure.

Keywords: charged colloids; charge reversal; surface charge amplification

1. Introduction

The electric double layer term denotes the arrangement of free ions around a usually charged colloid or surface immersed in an electrolyte. As it is well known, such a charge distribution plays a fundamental role in the physical chemistry of macromolecules since it determines most of the static and dynamic properties of colloidal dispersions [1,2]. A notable example of that is the recently found connection between the self-assembly process of a viral capsid (e.g., for the cowpea chlorotic mottle virus) and the neutralisation of its internal protein sub-units due to the charges of the enclosed RNA [3]. In the past decades, significant scientific efforts have been dedicated to develop an adequate picture of the electric double layer. Theoretical models have evolved from simple representations based on dimensionless, or punctual, electrolytic ions to more sophisticated ones including, for example, ion correlations, ionic excluded volume effects, image charges and solvation energies [4–13]. In particular, a decisive effect that has been successfully incorporated in the latest analysis of the electric double layer is that coming from the finite size of the ions. As a consequence of the gradual refinement of different models, a more faithful description has been achieved and a new phenomenology has been

uncovered. Notably, two peculiarities have been described in recent times: charge reversal and surface charge amplification [13–20]. The phenomenon of charge reversal is related to the local overcompensation of the bare colloidal charge by opposite-charged ions (or counterions) when the colloid is immersed in an electrolytic bath [19,21]. The adsorption of like-charged ions (or coions) on the surface of weakly charged macroions is the so-called surface charge amplification. In this last instance, the first layer of adsorbed coions amplifies the bare colloidal charge of macroions without the additional inclusion of specific interactions [19,21]. At present, there is an increasing and broad-based interest in the literature about the sequels and possible applications of these anomalies in a wide spectrum of situations in physics, chemistry, biology and technology (for representative examples of charge reversal and surface charge amplification in coagulation, biomolecular folding, ion channels, peptide titration and microfluidics, see Refs. [22–27]).

During the emergence of modern models and approaches to improve the description of the electric double layer, it was widely believed that these charge peculiarities, i.e., charge reversal and surface charge amplification, were totally absent from pioneering point-ions treatments based on the Poisson–Boltzmann equation. In other words, in the

*Corresponding author. Email: givan@ifisica.uaslp.mx

past, it was thought that charge reversal and surface charge amplification were exclusive of schemes including sized ions. However, this belief has been proved to be incorrect in recent years. Specifically, in 2006, Yu *et al.* [28] employed the unequal-radius modified Gouy–Chapman (URMGC) theory to investigate the electric double layer of *semi-punctual* ions for an electrified slit. These semi-punctual ions have a dual behaviour: they interact as charged points among them, whereas they interact as hard size-asymmetric spheres with the infinite plates. Note that this idealised electrolyte is different from the ‘de-ionised primitive model’ used in the past by several authors [29–31] to represent, for instance, a mixture of ‘unhydrated’ point ions interacting consistently with ‘hydrated’ hard-core ions in the primitive model. To our best knowledge, Yu *et al.*’s study was the first work that showed the above irregularities of the charge in a description founded on the classical Poisson–Boltzmann equation. In a subsequent study, some of the present authors [18] reported the appearance of surface charge amplification for an isolated spherical macroparticle in the presence of size-asymmetric semi-punctual ions. These semi-punctual results were in qualitative agreement regarding primitive model Monte Carlo simulations and integral equations calculations for very weakly charged colloidal particles in dilute supporting electrolytes. In particular, the phenomena of charge reversal and charge amplification in the Helmholtz zone, which are in the focus of this work, exhibited a similar qualitative behaviour in the semi-punctual and primitive models of the electric double layer in the very low-charge regime. Despite these findings, a comprehensive explanation of the origin of charge reversal and surface charge amplification in a mean-field description was not provided in any of these studies.

Apart from Refs [18,28], up to now, no other semi-punctual mean-field treatment of ions has examined the phenomena of charge reversal and surface charge amplification in colloidal systems. Thus, currently, there is a lack of a detailed survey of these phenomena for electric double layers of fully asymmetric semi-punctual ions in simple and/or relevant geometries, such as the spherical one. This issue is very appealing because the URMGC approach of fully asymmetric semi-punctual ions is a simple and relatively easy-to-solve theory, capable of displaying charge reversal and surface charge amplification. Moreover, it can be used to explain, at least in part, the origins of this colloidal phenomenology and/or serve as a basis for improved analysis. Precisely, the aim of this work is to provide a careful investigation of charge reversal and surface charge amplification, at the level of a fully asymmetric semi-punctual ions approach, for the very significant case of a spherical colloid. In this paper, a fresh reformulation of the URMGC theory in terms of an integral equation is exposed. Remarkably, we have addressed the scantily studied case of size- and charge-asymmetric electrolytes. The resulting data are used to characterise the phenomena of charge reversal and

surface charge amplification. We explore their zones of occurrence and assess the impact of several parameters of the system.

2. Model system and theory

The original Poisson–Boltzmann theory of the electric double layer was founded on the assumption of electrolytic point ions. This approach was used in the Gouy–Chapman (GC) theory to describe the ionic cloud surrounding an infinite planar electrode. Afterward, a distance of closest approach (unique for all the electrolytic species present) was incorporated to the treatment, giving rise to the modified Gouy–Chapman (MGC) formalism. This means that a theory of semi-punctual ions has been used since the advent of the MGC theory. However, it is a renowned fact that any of the structural functions associated to the GC and MGC theories (viz., the radial distribution functions, $g_i(r)$, the mean electrostatic potential, $\psi(r)$, or the integrated charge, $Q(r)$) exhibits always a monotonic behaviour. For the precise definition of $\psi(r)$ and $Q(r)$ in terms of the $g_i(r)$, see Equations (12) and (13). In particular, the integrated charge quantifies the accumulated charge coming from the macroparticle plus the ions contained in a spherical volume of radius r centred on the spherical colloid. This integrated charge is a very useful function that characterises the screening in the electric double layer and, for our purposes, represents a central quantity since the condition $Q(r)Q_0 < 0$, where Q_0 is the bare colloidal charge, indicates the phenomenon of charge reversal, whereas the pair of conditions $Q(r)Q_0 > 0$ and $|Q(r)| > |Q_0|$ implies surface charge amplification. In the case of the GC and the MGC theories, the integrated charge goes invariably to zero, i.e., without changes of sign or maxima/minima, showing that the double layer of either punctual ions or semi-punctual ions with equal ‘radii’ neutralises monotonically the colloidal charge, that is, the phenomena of charge reversal and surface charge amplification do not occur in the GC and the MGC formalisms.

Years later, the use of different closest approach distances between ions and colloids was proposed to improve the accuracy of the MGC approach. This theory was termed as the URMGC theory and was introduced by Torrie and Valleau in the early 1980s to describe the ion distribution around an infinite charged plate [32]. The solution of the corresponding differential equation displayed a non-monotonical comportment of the ionic profiles and the associated mean electrostatic potential (see, e.g., Figure 5 in Ref. [32]). As mentioned in the Introduction, such oscillating radial distribution functions and mean electrostatic potential profiles were unexpected in the URMGC theory since, previously, such behaviour had been observed exclusively in ion-sized treatments [14,33]. On the other side, it is remarkable that the inaugural URMGC article by Torrie and Valleau did not explore the integrated charge profiles. Thus, the phenomena of charge reversal and

surface charge amplification passed unnoticed. Instead of examining the integrated charge, in Ref. [32] another noticeable event was exposed, the so-called *dominance of the counterions*. Citing the authors: ‘... Consider in particular the case of a *strong electrical field* (of either sign) at the surface. In this limit, only *counterions* will be found near the surface, and the only important ion-size parameter will be the effective radius of the counterion...’, which suggested compellingly that there was no real importance in considering different distances of closest approach between the ions and the colloid for *high* surface charges. Unfortunately, such asseveration, rigorously valid for the Poisson–Boltzmann equation at *large fields*, diminished the interest in the URMGC theory and discouraged its use for many years. The latency of this size-asymmetric semi-punctual ions theory was broken by the aforementioned paper by Yu *et al.* [28], who solved semi-analytically the Poisson–Boltzmann differential equation for a binary electrolyte in and out a planar slit. These authors also calculated explicitly the integrated charge, uncovering the phenomena of charge reversal and surface charge amplification in semi-punctual-ions models in planar geometry. In this context, we are here interested in the theoretical description of the ionic structure around a spherical macroion, with special emphasis on the integrated colloidal charge, in the framework of a semi-punctual-ions mean-field approach. Our main goal is to analyse and explore detailedly the phenomena of charge reversal and surface charge amplification in this relevant geometry.

The system under study consists of a binary electrolyte bathing a unique spherical colloid. Particularly, in our model the colloid is taken as a hard sphere of radius R , with a uniform surface charge density σ_0 . The ionic species in the electrolyte are considered as *semi-punctual* charges

with ‘radius’ r_i dissolved in a continuous solvent. As usual, all the system is supposed to be an electroneutral assembly of charges. For simplicity, and to avoid image charge effects, the same value of the dielectric constant, ϵ , is assumed in the whole space. Specifically, the ion–ion spherically symmetric interactions for the two electrolytic species are then given by

$$U_{ij}(r) = \frac{z_i z_j e^2}{\epsilon r}, \quad r > 0, \quad (1)$$

where $i, j = 1, 2$, z_i are the ionic valences and e is the *protonic* charge, whilst the colloid-ion potentials are

$$U_{Mj}(r) = \begin{cases} \infty, & r < R + r_j, \\ \frac{z_M z_j e^2}{\epsilon r}, & r \geq R + r_j, \end{cases} \quad (2)$$

where the index M denotes the macroparticle or colloid, $j = 1, 2$, and $Q_0 = z_M e = 4\pi R^2 \sigma_0$ is the native or bare colloidal charge. Note that the main premise in our URMGC approach establishes that the ionic distances of closest approach to the colloidal surface, r_1 and r_2 , can be different.

For convenience, and instead of using the typical identification of the two ionic species ($i, j = 1, 2$) as cations (+) and anions (–), without loss of generality, herein we will just discern between one species of small ions with index s , and another one formed by big ions with index b . Both species fulfil the condition $z_s z_b < 0$. In terms of the closest approach distances, we then have that $r_s \leq r_b$. Accordingly, in the rest of the paper, the notation with indexes s and b for the ionic species will be adopted. A diagram of the model system can be seen in Figure 1.

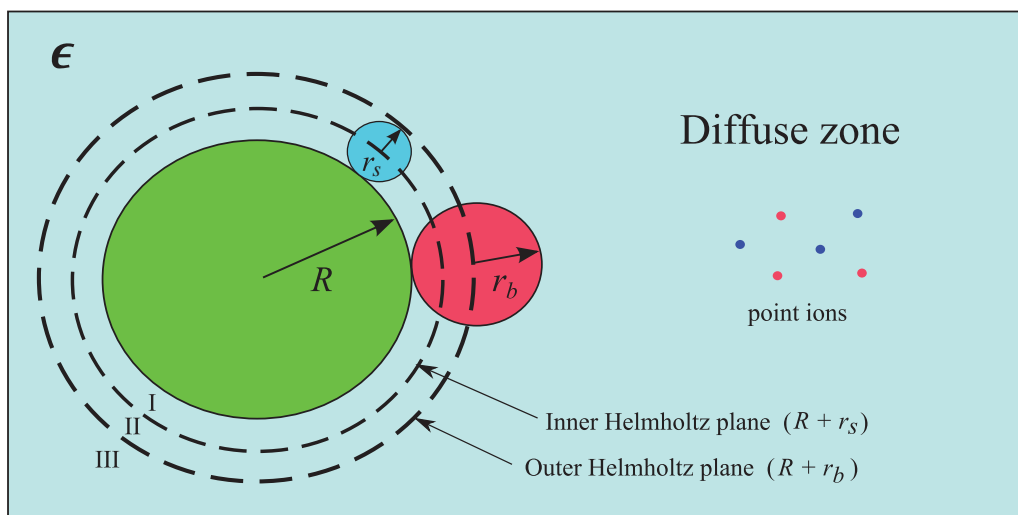


Figure 1 Schematic representation of the size-asymmetric semi-punctual electric double layer. The *Helmholtz zone* comprises the region II, limited by the inner and outer Helmholtz planes. Note the conventional use of the term ‘plane’.

The usual manner to determine the structure of our electric double layer should be starting from the Poisson–Boltzmann differential equation for the mean electrostatic potential, $\psi(r)$, and solve it for the appropriate boundary conditions, i.e., considering different distances of closest approach for cations and anions. This has been the path employed previously in Refs [28,32,34–36]. Rather, a different venue is followed here, in which we will recast the URMGC theory for spherical symmetry in terms of an integral equation. In such an integral approach, the principal quantities are now the radial distribution functions, $g_{Ms}(r)$ and $g_{Mb}(r)$, of the small and big species around the macroparticle (identified by M).

In turn, the corresponding URMGC integral equation for the spherical electric double layer can be derived in two equivalent ways. In specific, the first one (or Version I) is based on the characteristic Poisson–Boltzmann relation:

$$g_{Mj}(r) = \exp[-z_j e \psi(r) / k_B T], \text{ for } r \geq R + r_j, \text{ and} \quad (3)$$

$$j = s, b,$$

with k_B being the Boltzmann's constant and T the absolute temperature, whereas the second option (or Version II) depends on the Ornstein–Zernike equation. Version I is perhaps the most direct route and basically consists in (1) writing the fundamental expression of the mean electrostatic potential in terms of an integral of the ionic radial distribution functions (see Equation (12)) and (2) substituting such expression in the right-hand side of Equation (3). Alternatively, the derivation of Version II is more illustrative and insightful, as it will be commented below, and proceeds as follows. We depart from the Ornstein–Zernike equation for the total correlation functions, $h_{kl}(\vec{r})$, namely:

$$h_{kl}(\vec{r}) = c_{kl}(\vec{r}) + \sum_m \rho_m \int h_{km}(\vec{t}) c_{ml}(\vec{s}) d\vec{t}^3, \quad (4)$$

where the indices k , l and m run for all the species of particles in the system, ρ_m is the bulk number density of each species, \vec{r} , $h_{kl}(\vec{r})$ and $c_{kl}(\vec{r})$ are the distance, total correlation function and direct correlation function, respectively, for two particles of types k and l , and something analogous for \vec{t} , $\vec{s} = \vec{r} - \vec{t}$, $h_{km}(\vec{t})$, and $c_{ml}(\vec{s})$.

In our case, we have an isolated colloid ($\rho_M \rightarrow 0$) at the origin and then, from Equation (4), we can decouple the following pair of spherically symmetric integral equations:

$$h_{Mj}(r) = c_{Mj}(r) + \sum_{m=s,b} \rho_m \int h_{Mm}(t) c_{mj}(|\vec{r} - \vec{t}|) dt^3, \quad (5)$$

$$\text{for } j = s, b.$$

Given that the total correlation functions and radial distribution functions are related by $h_{Mi}(r) = g_{Mi}(r) - 1$, Equation (5) must be supplemented with two closures to end up with

a solvable set of equations. Concretely, for the colloid ion, we use the hypernetted chain (HNC) relation:

$$c_{Mj}(r) = -\beta U_{Mj}(r) + h_{Mj}(r) - \ln(h_{Mj}(r) + 1), \quad (6)$$

$$\text{for } j = s, b,$$

which is a well-established approximation in Coulombic fluids, and for the ion–ion we choose the Debye–Huckel (DH) one:

$$c_{ij}(r) = -\beta U_{ij}(r), \text{ for } i, j = s, b. \quad (7)$$

In the above equations, $\beta = 1/k_B T$. Substitution of Equations (6) and (7) in Equation (5) then leads to the HNC/DH integral equations for the spherical electric double layer of semi-punctual ions with different distances of closest approach:

$$g_{Mj}(r) = \exp \left[-\beta z_j e \left(\frac{4\pi R^2 \sigma_0}{\epsilon r} + \sum_{m=s,b} \rho_m z_m e \int \frac{g_{Mm}(t)}{\epsilon |\vec{r} - \vec{t}|} d^3 t \right) \right], \text{ for } j = s, b. \quad (8)$$

The integration of variables θ and ϕ in the right-hand side of Equation (8) can be accomplished analytically and, after some algebra, we arrive to the following non-dimensional expressions, which are particularised for the different spatial regions (see Figure 1):

Region I:

$$g_s(r') = g_b(r') = 0, \text{ for } 1 \leq r' < 1 + \gamma_s. \quad (9)$$

Region II:

$$g_s(r') = \exp \left[\frac{1}{r'} [A + B(X(r') + r'N)] \right], \quad (10)$$

$$\text{for } 1 + \gamma_s \leq r' < 1 + \gamma_b,$$

with $g_b(r') = 0$, $X(r') = \int_{1+\gamma_s}^{r'} g_s(t') t'^2 dt' + \int_{r'}^{1+\gamma_b} g_s(t') t' r' dt'$, and

$$N = \int_{1+\gamma_b}^{\infty} \{g_s(t') - [g_s(t')]^\lambda\} t' dt'.$$

Region III:

$$g_s(r') = \exp \left[\frac{1}{r'} [A + B(Y + Z(r'))] \right], \text{ for } 1 + \gamma_b \leq r' < \infty, \quad (11)$$

$$\text{with } g_b(r') = [g_s(r')]^\lambda, Y = \int_{1+\gamma_s}^{1+\gamma_b} g_s(t') t'^2 dt', \text{ and}$$

$$Z(r') = \int_{1+\gamma_b}^{r'} \{g_s(t') - [g_s(t')]^\lambda\} t'^2 dt'$$

$$+ r' \int_{r'}^{\infty} \{g_s(t') - [g_s(t')]^\lambda\} t' dt'.$$

Note that in the previous equations a normalised form has been adopted, where we have introduced the reduced distances $r' = r/R$ and $t' = t/R$ and the parameters $\gamma_s = r_s/R$, $\gamma_b = r_b/R$, $\lambda = z_b/z_s$, $A = -(4\pi\beta R z_s e \sigma_0)/\epsilon$ and $B = -(4\pi\beta R^2 \rho_s z_s^2 e^2)/\epsilon$. To simplify the notation, we have suppressed the subindex M in the $g_s(r)$ and $g_b(r)$ functions. Even though Equations (9)–(11) were implicitly used in Ref. [18], we present here their detailed forms. After resolving this set of equations for $g_s(r)$ and $g_b(r)$, other physical properties can be obtained. For example, the mean electrostatic potential and integrated charge can be calculated from the radial distributions via the integrals:

$$\psi(r) = \frac{4\pi R^2 \sigma_0}{\epsilon r} + \sum_{m=s,b} \rho_m z_m e \int \frac{g_{Mm}(t)}{\epsilon |\vec{r} - \vec{t}|} d^3t \quad (12)$$

and

$$Q(r) = 4\pi R^2 \sigma_0 + \sum_{m=s,b} 4\pi \rho_m z_m e \int_R^r g_{Mm}(t) t^2 dt. \quad (13)$$

The integrated charge, $Q(r)$, will be used in the next section as the chief indicator of charge reversal and surface charge amplification in the spherical electric double layer of semi-punctual ions.

The complete equivalence between the two routes, Versions I and II, to obtain the integral equations representation can be easily demonstrated using Equations (3), (8) and (12). In other words, the HNC/DH expressions of Equations (9)–(11) are the explicit integral form of the URMGC theory for the spherical electric double layer of fully size- and charge-asymmetric semi-punctual ions. This scheme complements the ordinary differential equations formalism of the URMGC theory, originally proposed for the planar geometry, which is usually solved in terms of the mean electrostatic potential [28,32,34–36].

Before ending this section, we would like to point out that our preference for the deduction of Version II was supported by three reasons, namely (1) the integral equations route represents a novel way to pose the URMGC theory starting from fundamental principles of the statistical mechanics of liquids, (2) the resulting system of equations for the radial distribution functions is solvable accurately by means of robust numerical methods and, more importantly, (3) this derivation is fruitful since it enlightens the connection between the URMGC theory and surpassing ways

to improve such formalism by embodying ionic finite size effects and ion–ion correlations. Specifically, if the point-ions supposition of Equation (7) is substituted by a non-punctual closure (e.g., the mean spherical approximation (MSA) or the HNC relation), an enhanced treatment of the asymmetric spherical electric double layer can be obtained [17,18].

The actual determination of the URMGC radial distribution functions, $g_s(r)$ and $g_b(r)$, was performed by means of an iterative numerical solution of the system of Equations (9)–(11). An efficient Picard method was used to calculate the corresponding ionic profiles. A Simpson's rule integration of the radial distribution functions, $g_i(r)$, in Equation (13) rendered the integrated charge, $Q(r)$. The numerical solution of the system of coupled integral equations defined by Equations (9)–(11) used typically a grid of 10 points per radius of the smallest ionic species. In order to avoid additional numerical errors, the mean electrostatic potential, $\psi(r)$, was obtained directly from the logarithm of Equation (3). Computational details can be found elsewhere [13,37,38].

3. Results and discussion

We have solved the URMGC integral equation in spherical geometry for a wide range of size-asymmetric binary electrolytes, with symmetry and asymmetry in charge, around a colloid of varying radius, R , and surface charge density, σ_0 . For definitiveness, we have considered $\sigma_0 \geq 0$, since the situation of a negatively charged macroparticle is covered by the corresponding interchange of signs of the valences z_s and z_b . The temperature and dielectric constant in all the systems studied were $T = 298$ K and $\epsilon = 78.5$, respectively. The following convention was adopted in order to facilitate the identification of the size and charge of the ionic species involved in each case of study: when the valences of a binary electrolyte be specified by the notation n,m , the symbols n and m will be associated to the smallest and largest species, respectively.

In the following paragraphs, we discuss data for (1) charge-symmetric and (2) charge-asymmetric electrolytes. We must point out that the latter case has been scarcely examined in the literature.

3.1. Size-asymmetric $z_s z_b$ charge-symmetric electrolytes

In Figure 2, we display data for the integrated charge, $Q(r')$, in $-1: +1$ systems. Therein, the electrolyte bulk concentrations are $\rho_s = \rho_b = 1M$. The three graphs in the upper row (Figure 2(a)–(c)) display results for three different combinations of r_s and r_b , and for a macroparticle of radius $R = 10$ Å with a varying surface charge density σ_0 . Meanwhile, in the lower row (Figure 2(d)–(f)), we have the same combinations of ionic closest approach distances but for a larger

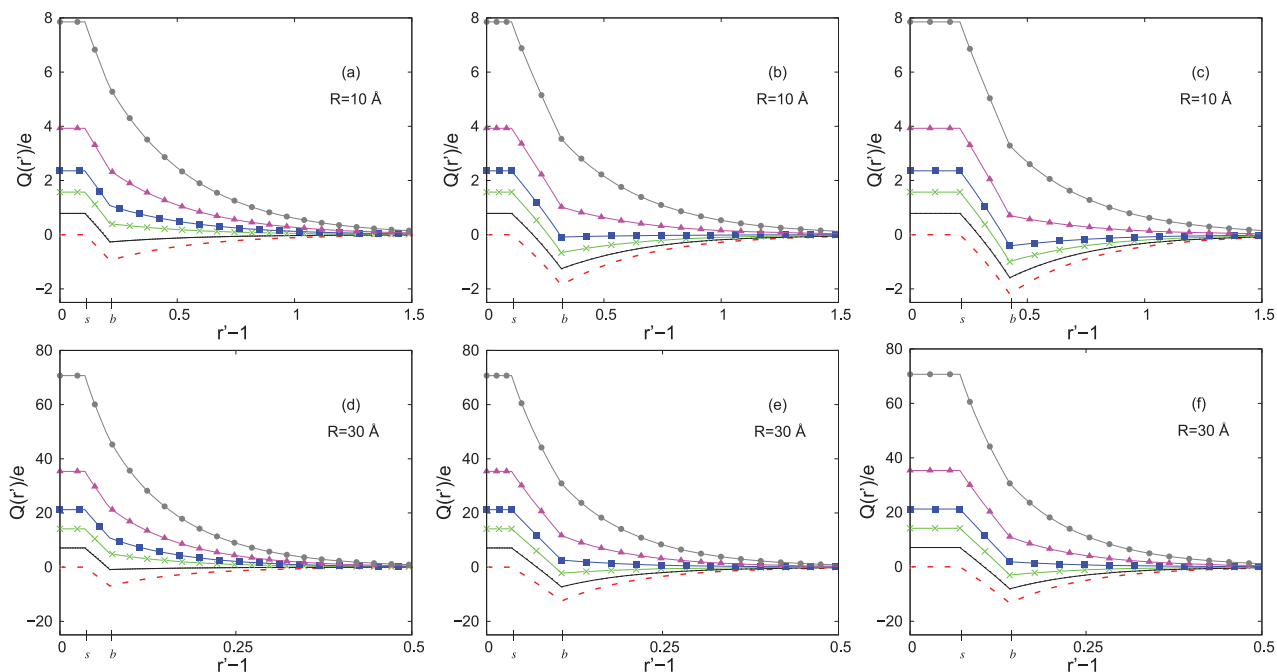


Figure 2 Integrated charge, $Q(r')$, around a macroion as a function of the distance to its surface. The charged colloid is immersed in a size-asymmetric $-1: +1$, 1 M electrolyte. The dashed, solid, solid-crosses, solid-squares, solid-triangles and solid-circles lines correspond to the surface charge densities $\sigma_0 = 0, 0.01, 0.02, 0.03, 0.05$ and 0.1 C/m², respectively. The ionic ‘radii’ are denoted as r_s and r_b for the smallest and the biggest ionic species, respectively. The corresponding values used in each panel are: (1) $r_s = 1.0625$ Å and $r_b = 2.125$ Å in (a) and (d); (2) $r_s = 1.0625$ Å and $r_b = 3.1875$ Å in (b) and (e); and (3) $r_s = 2.125$ Å and $r_b = 4.25$ Å in (c) and (f). The radius of the macroion in the top row and in the bottom row are 10 and 30 Å, respectively.

colloid of radius $R = 30$ Å with the same surface charge densities of the smallest colloid. A global examination of Figure 2(a)–(f) leads to the following three main findings. (1) As soon as an initially neutral colloid acquires a charge, the phenomenon of charge reversal arises. (2) In each panel of Figure 2, the curves of the integrated charge $Q(r')$ for different values of the colloidal surface charge density, σ_0 , never cross each other. For that reason, when the magnitude of the colloidal charge is gradually increased, there will be always a critical value, $\sigma_0^{\text{critical}}$, for which the charge reversal disappears. (3) The integrated charge $Q(r')$ experiences a change of its sign at a distance that is invariably situated in the Helmholtz region, i.e., the onset of the charge reversal ($Q_0 Q(r') < 0$) occurs unfailingly in the spatial interval $(1 + \gamma_s, 1 + \gamma_b]$. Summarising (1)–(3), for a $-1: +1$ electrolyte with small counterions, charge reversal is always present, albeit it is limited to happen in a finite interval of macroparticle charges $(0, \sigma_0^{\text{critical}}]$, whereas its onset is spatially *localised* inside the Helmholtz zone. Beyond the outer Helmholtz surface ($r' > 1 + \gamma_b$), the event of a reversion in the sign of the integrated charge $Q(r')$ is totally absent. Besides, no surface charge amplification was detected under any circumstance.

A collateral phenomenon also noticeable in Figure 2 is that, for systems where charge reversal exists, the integrated charge beyond the Helmholtz region ($r' > 1 +$

γ_b) behaves as one corresponding to an ‘inversely charged’ macroparticle. In other words, the net total charge of the complex formed by the colloid plus the adjacent counterions is reversed, a condition that surely implies a change in the roles of the anions and cations in the external double layer (see the discussion about ionic density profiles below). This phenomenon has been extensively discussed in the literature [16,23,39] and could have remarkable sequels in the electrokinetic behaviour of charged colloidal particles.

Charge reversal for univalent electrolytes exhibits diverse particularities when specific parameters are changed. For instance, in Figure 2(a) and 2(b), we observe that, for a fixed ‘size’ of the small counterions, a larger ratio between the ionic closest approach distances, r_b/r_s , that also implies the augmentation of the difference $r_b - r_s$, enhances the charge reversal (e.g., the minimum values of the integrated charge for $\sigma_0 = 0.01$ C/m², at $r' = 1 + \gamma_b$, are $-0.267e$ and $-1.258e$ in Figure 2(a) and 2(b), respectively). On the other hand, Figure 2(a) and 2(c) shows that, for a constant ratio r_b/r_s , an increment in the ionic closest approach distance for counterions, with the consequent enlargement of $r_b - r_s$, induces a stronger charge reversal (note that in Figure 2(c) the minimum of $Q(r')$ for $\sigma_0 = 0.01$ C/m², at the outer Helmholtz surface or at $r' = 1 + \gamma_b$, is $-1.589e$). Concomitantly, for a given difference $r_b - r_s$ between the ionic ‘sizes’ (Figure 2(b) and 2(c)), an augmentation in

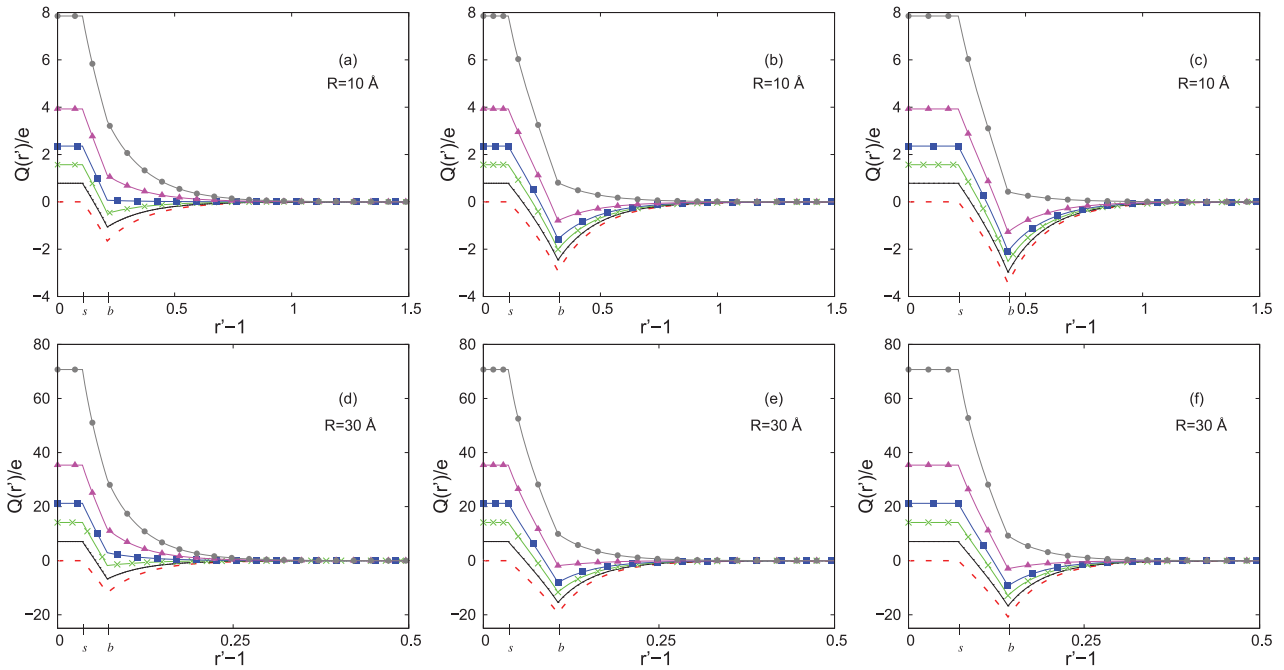


Figure 3 Integrated charge, $Q(r')$, around a macroion as a function of the distance to its surface. The charged colloid is immersed in a size-asymmetric $-2: +2$, 1 M electrolyte. The parameters of the different systems portrayed and the convention of symbols are the same as those used in Figure 2.

the magnitude of the ionic closest approach distance of the smallest ions results in a major charge reversal.

With respect to the influence of the macroparticle radius, we notice that, in the lower panel of Figure 2(d)–(f), the magnitude of $Q(r')$ is larger due to the fact that its value at the surface depends quadratically on R (i.e., $Q_0 = 4\pi R^2 \sigma_0$). As a result, the intensity of the charge reversal is strengthened for the biggest colloid ($R = 30 \text{ \AA}$). To compare with the upper row, in Figure 2(d)–(f), for $\sigma_0 = 0.01 \text{ C/m}^2$, at $r' = 1 + \gamma_b$, the minimum values of the integrated charge are $-0.888e$, $-7.284e$ and $-8.112e$, respectively.

The consequences of varying the ionic valence can be seen in Figure 3, where we portray results for $-2: +2$ electrolytes, keeping constant the rest of the parameters employed in Figure 2. A consideration of Figure 3 vis-à-vis Figure 2 confirms the chief conclusions derived from data for univalent electrolytes, namely (1) the persistence of charge reversal for systems with small counterions and its existence in a finite interval of colloidal charge ($0, \sigma_0^{\text{critical}}$] and (2) the starting of the charge reversal is also constrained to the Helmholtz zone ($1 + \gamma_s, 1 + \gamma_b$]. However, due to the enhanced charge reversal for divalent ions, two additional characteristics can be noticed in these $-2: +2$ cases: first, the span of macroparticle surface charges for which charge reversal appears is increased, i.e., we have larger values of $\sigma_0^{\text{critical}}$, and, second, the extent of the double layer is visibly shortened. Again, appropriate changes in the ionic closest approach distances (see Figure 3(a)–(c)

or, else, Figure 3(d)–(f) or in the colloidal radius (compare upper and lower rows in Figure 3) have analogous effects on charge reversal as those seen in univalent electrolytes. In specific, for $\sigma_0 = 0.01 \text{ C/m}^2$, $Q(r' = 1 + \gamma_b)$ has the values $-1.060e$, $-2.455e$ and $-2.968e$, for Figure 3(a)–(c) in the upper row, respectively, whilst it has the values $-6.762e$, $-15.427e$ and $-16.711e$, for Figure 3(d)–(f) in the lower row, respectively.

The distinct compartments of charge reversal revealed in Figures 2 and 3 can be nicely rationalised in terms of several structural arguments. Starting from the definitions of the mean electrostatic potential and the integrated charge (Equations (12) and (13), respectively), rather straightforward differentiations lead to the next general relationships for the spherical electric double layer:

$$Q(r') = -\epsilon R r'^2 \frac{d\psi(r')}{dr'} \quad (14)$$

and

$$\frac{dQ(r')}{dr'} = 4\pi R^3 r'^2 \rho_c(r'), \quad (15)$$

where $\rho_c(r') = \rho_s z_s e (g_s(r') - g_b(r'))$ is the local charge density. In the equation for $dQ(r')/dr'$ above, notice the discontinuity of $\rho_c(r')$ at $r' = 1 + \gamma_b$. Equation (14) and similar relations for other geometries have been given elsewhere [15,38,40].

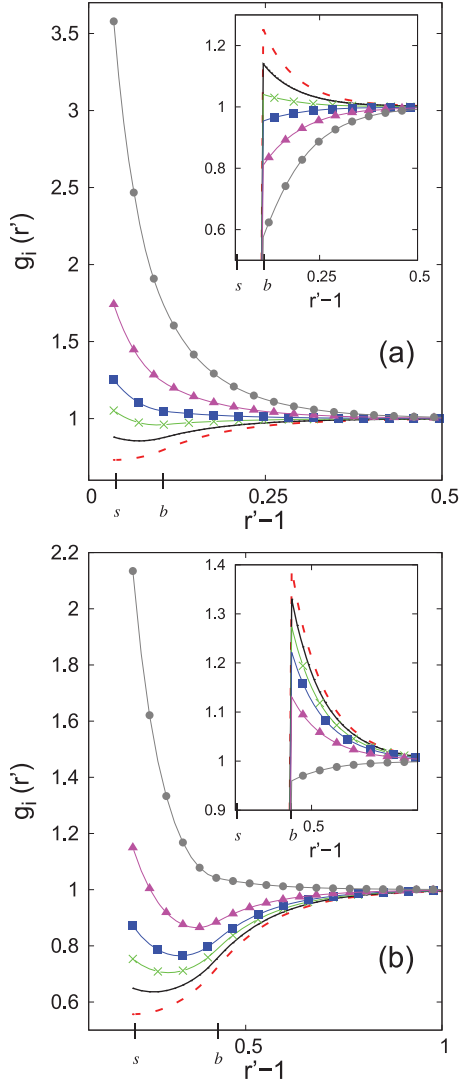


Figure 4 Radial distribution functions of monovalent and divalent size-asymmetric $z: z$ ions around a macroion for different surface charge densities. In panel (a), the macroion has a radius $R = 30 \text{ \AA}$ and it is immersed in a $-1: +1, 1 \text{ M}$ electrolyte with ionic ‘radii’ $r_s = 1.0625 \text{ \AA}$ and $r_b = 3.1875 \text{ \AA}$. In panel (b), the macroion has a radius $R = 10 \text{ \AA}$ and it is immersed in a $-2: +2, 1 \text{ M}$ electrolyte with ionic ‘radii’ $r_s = 2.125 \text{ \AA}$ and $r_b = 4.25 \text{ \AA}$. The correspondence between lines and surface charge densities is the same as that used in Figure 2.

For the URMGC theory, and making use of the Boltzmann form of $g_s(r')$, Equation (14) can be recasted as

$$Q(r') = \frac{\epsilon R}{z_s e \beta} r'^2 \frac{1}{g_s(r')} \frac{dg_s(r')}{dr'}. \quad (16)$$

Alternatively, based on the electroneutrality condition, we can rewrite Equation (14) as follows:

$$Q(r') = -4\pi R^3 \int_{r'}^{\infty} \rho_c(t') t'^2 dt'. \quad (17)$$

Thus, Equations (14) and (16) indicate that any change of sign of $Q(r')$ must occur at positions where the $g_s(r')$ and $\psi(r')$ functions have their maxima/minima. In Figures 2 and 3, we observe that, for systems undergoing charge reversal, the integrated charge passes by zero only once. Also notice that the initial reversion of sign always happens between the inner and outer Helmholtz surfaces, that is, in the region $1 + \gamma_s < r' \leq 1 + \gamma_b$. This indicates that the origin of this phenomena can then be attributed to the oscillatory behaviour, and the associated extremum, of the $g_s(r')$ and $\psi(r')$ functions in the Helmholtz zone. To illustrate that, in Figure 4 the ionic profiles for representative $-1: +1$ and $-2: +2$ instances are displayed. Therein, we corroborate the occurrence of an oscillatory compartment and the existence of a minimum in the $g_s(r')$ inside the Helmholtz region, as well as its posterior monotonic approach to zero in the external double layer (i.e., for $r' \geq 1 + \gamma_b$). This spatial variation of the curves in Figure 4 is reflected in the integrated charge graphs of Figures 2 and 3, and then explains the whole development of the charge reversal phenomenon. Additionally, Equation (17) allows us to connect the integrated charge and the local charge density. On these grounds, we realise that the smooth tendency of the integrated charge $Q(r')$ to zero outside the Helmholtz zone is just a consequence of the monotonic and one-signed behaviour of $\rho_c(r')$ there. To explain it better, we note that, since, for $r' > 1 + \gamma_b$, $g_s(r')$ and $g_b(r')$ go monotonically to 1 without any intersection between these two ionic profiles, the charge density $\rho_c(r')$ must then be a non-fluctuating and one-signed function in the diffuse double layer. Hence, a simple application of the additivity-with-respect-to-intervals and monotonicity properties of an integral [41] to the right-hand side of Equation (17) proves that the integrated charge must tend steadily to zero or, equally, that the *punctual* ionic atmosphere beyond the Helmholtz zone neutralises in a gradual form the net charge enclosed by the outer Helmholtz plane. Then again, according to Equation (15) the rate of change of $Q(r')$ depends directly from the value of $\rho_c(r')$. In Figure 4 we observe that, for $1 + \gamma_s \leq r' < 1 + \gamma_b$, $g_s(r')$ is always positive, whereas, for distances beyond the Helmholtz zone, $g_s(r')$ and $g_b(r')$ never cross each other, from which the *derivative* of $Q(r')$ must be a non-zero function with a constant sign in each one of the two intervals $[1 + \gamma_s, 1 + \gamma_b)$ and $(1 + \gamma_b, \infty)$, but with opposite sign because of the electroneutrality condition. Equivalently, the integrated charge does not oscillate, nor has extrema, either in the interior of the Helmholtz zone or in the exterior part of the double layer.

In recent literature, there is a handful of theories for the electric double layer [17,18,38,40,42–45], e.g., the HNC/MSA integral equation for the spherical double layer, that recurrently predict integrated charges with a non-monotonic behaviour and with multiple occasions of charge reversal. Those more sophisticated formalisms include

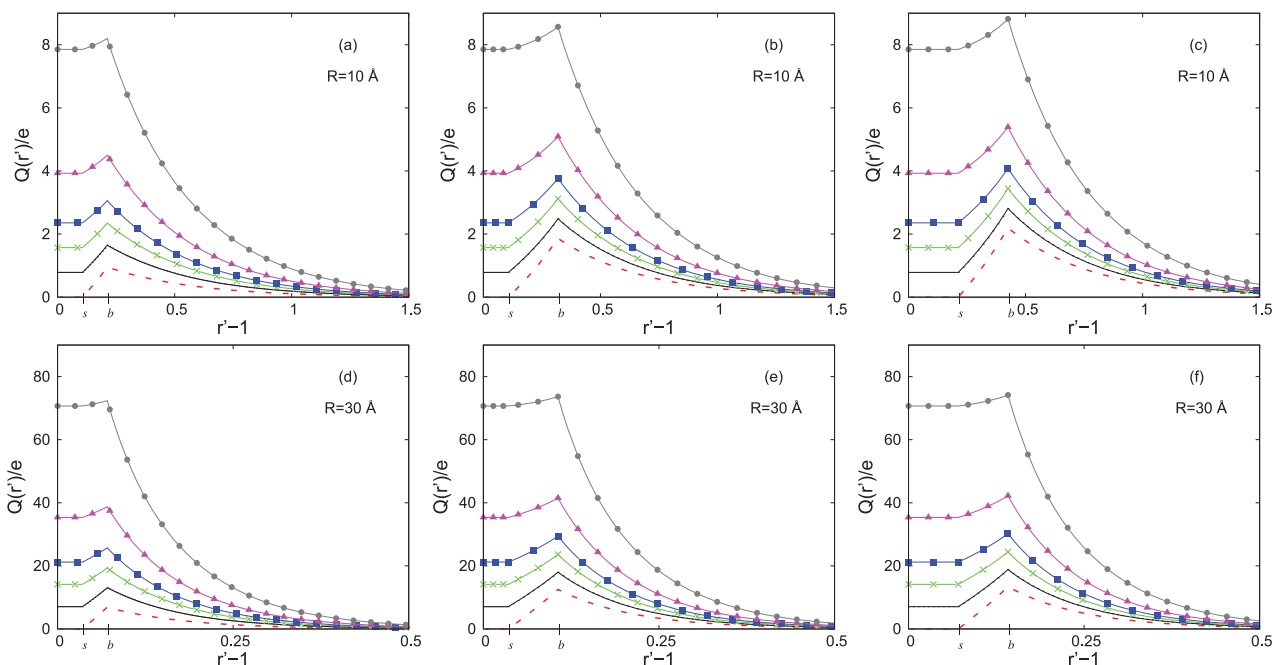


Figure 5 Integrated charge, $Q(r')$, around a macroion as a function of the distance to its surface. The charged colloid is immersed in a size-asymmetric $+1: -1, 1$ M electrolyte. The parameters of the different systems portrayed and the convention of symbols are the same as those used in Figure 2.

effects, like ion correlations and ionic excluded volume effects, that are not present in our mean-field approach. In physical terms, these improvements in the treatment of the electric double layer are performed by using the so-called primitive model of an electrolyte, in which it is supposed that ions are genuine spheres of finite size. Under such circumstances, those theories have proven that charge reversal can occur everywhere in the double layer. Contrastingly, the foregoing discussion established that the integrated charge in the semi-punctual URMGC formalism will be inevitably a non-oscillatory function before and after the outer Helmholtz plane, with a unique discontinuous derivative at $r' = 1 + \gamma_b$ (where the outer Helmholtz plane is defined). Thus, we conclude that, for small counterions, the maximum charge reversal observed in the regime of non-high colloidal surface charge is unique and is situated precisely at the outer Helmholtz plane. Note that this extremum and the concomitant onset of the charge reversal (when the condition $Q(r')Q_0 < 0$ sets in) are restricted to lie between the inner and outer Helmholtz planes. All these facts illustrate the *localisation* of these effects in the Helmholtz zone. Interestingly, note that such charge reversal present inside the Helmholtz zone for $\sigma_0 > 0$ can be also associated to a ‘negative’ macroion if one is only able to detect the ions that are outside the Helmholtz zone. In such a scenario, cations act as counterions and anions as coions.

In a nutshell, in the URMGC approach, the occurrence and compartment of the charge reversal and the localisation of its onset and its maximum magnitude between the Helmholtz planes are completely dictated by the possi-

ble non-monotonic conduct of $g_s(r')$ in the interior of the Helmholtz zone, on the one hand, and by the monotonicity of the two radial distribution functions in the diffuse electric double layer, on the other.

We now turn our attention to the case of spherical electric double layers with small coions. For systems with non-negatively charged colloids, as those considered here, we should be dealing with little cations. Given their minor closest approach distance, the coions are the only species present in the Helmholtz region, which induces the appearance of surface charge amplification. Figures 5 and 6 depict the corresponding integrated charge for $+1:-1$ and $+2:-2$ systems with similar macroparticle radii and combinations of closest approach distances to those used in Figures 2 and 3. On the whole, the integrated charge $Q(r')$ graphs for univalent and divalent electrolytes in Figures 5 and 6 evidence the following main features. (1) Any colloidal charge different from zero produces the phenomenon of charge amplification. However, this time, and differently from the instance of small counterions, as the magnitude of σ_0 grows there is not a $\sigma_0^{\text{critical}}$ for which surface charge amplifications ceases. Consequently, we will be able to detect the amplification of the effective charge for every non-neutral macroparticle surrounded by coions that are smaller than counterions. (2) The intensity of the surface charge amplification effect diminishes uniformly with σ_0 . Using the difference $\Delta Q = |Q(r' = 1 + \gamma_b) - Q_0|$ as a measure of the surface charge amplification, we can see that ΔQ decreases gradually when the colloidal charge is enlarged [19]. (3) In each panel of Figures 5 and 6, we note that the

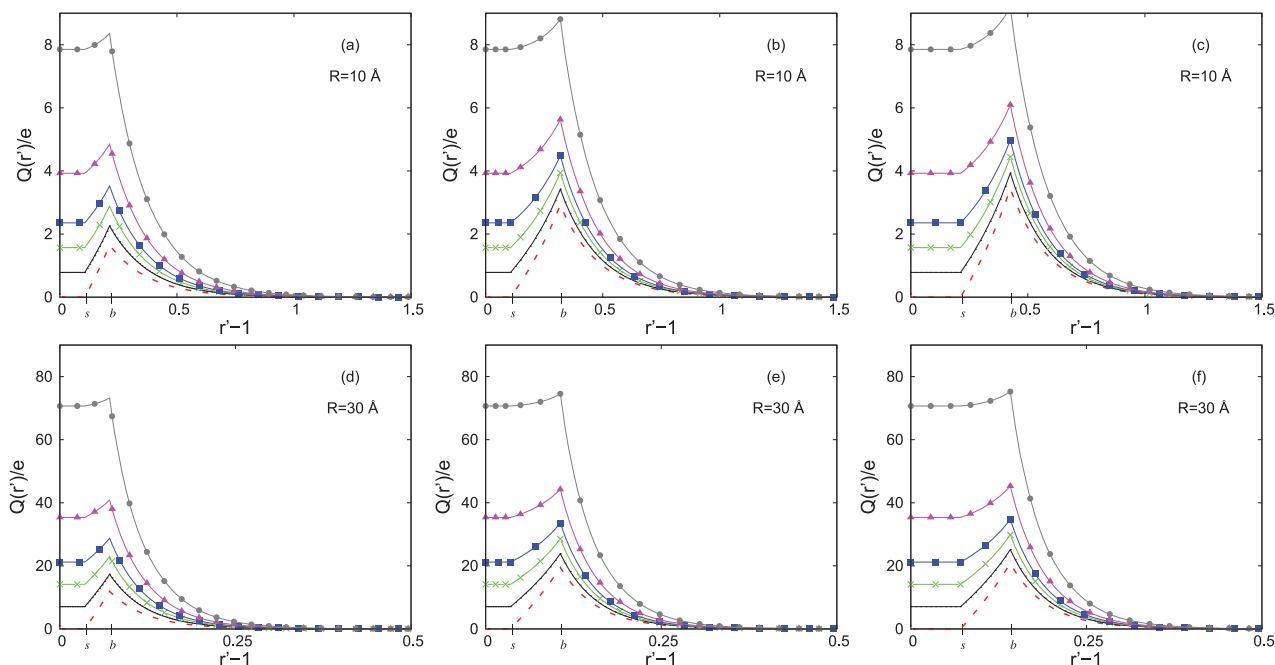


Figure 6 Integrated charge, $Q(r')$, around a macroion as a function of the distance to its surface. The charged colloid is immersed in a size-asymmetric $+2: -2, 1\text{ M}$ electrolyte. The parameters of the different systems portrayed and the convention of symbols are the same as those used in Figure 2.

$Q(r')$ curves for distinct σ_0 never intersect each other and that, as a function of the distance, apart from the peak at $r' = 1 + \gamma_b$, the integrated charge does not present spatial oscillations or local maxima/minima (points where its derivative $dQ(r')/dr'$ is zero). (4) The rise of the magnitude of $Q(r')$ and the maximum value of the surface charge amplification are always localised in the interval $[1 + \gamma_s, 1 + \gamma_b]$. (5) When coions are the species with the minor closest approach distance, charge reversal is never observed.

The distinct univalent systems portrayed in Figure 5 exemplify the typical behaviour of the surface charge amplification for variations in the ionic closest approach distances, colloidal radius and colloidal surface charge, similar to those used in Figures 2 and 3. Considering first the upper row ($R = 10\text{ \AA}$), a comparison between Figure 5(a) and 5(b) shows that the surface charge amplification phenomenon can be enhanced if, for a given value of r_s , the ratio r_b/r_s augments, enlarging also the difference $r_b - r_s$ (e.g., in Figure 5(a) and 5(b), the integrated charge $Q(r' = 1 + \gamma_b)$ has the values $1.647e$ and $2.485e$, respectively, for $\sigma_0 = 0.01\text{ C/m}^2$). If the ratio r_b/r_s is fixed but r_s and $r_b - r_s$ are allowed to increase, the surface charge amplification is also magnified (e.g., in Figure 5(a) and 5(c), the integrated charge $Q(r' = 1 + \gamma_b)$ has the values $1.647e$ and $2.812e$, respectively, for $\sigma_0 = 0.01\text{ C/m}^2$). Complementarily, when the difference between the ionic closest approach distances, $r_b - r_s$, is now kept constant (as in Figure 5(b) and 5(c)), a larger r_s leads to an intensification of the surface charge amplification.

On the other hand, if the radius of the macroparticle is changed to $R = 30\text{ \AA}$ (see lower row of Figure 5), for a given σ_0 , the integrated charge has values that can be around 10 times larger than those of $R = 10\text{ \AA}$ (by the same reasons argued in the discussion associated to Figure 2). Consequently, all the traits of the surface charge amplification observed in Figure 5(a)–(c) are emphasised in the lower row (for instance, $Q(r' = 1 + \gamma_b)$, for $\sigma_0 = 0.01\text{ C/m}^2$, is $13.077e$, $17.991e$ and $18.813e$, in Figure 5(d)–(f), respectively).

In Figure 6, we have considered the same combination of values for the radius of the macroion, electrolyte concentration and ionic closest approach distances used in Figure 5. However, in this case, we will assess the development of the surface charge amplification phenomenon for $+2:-2$ electrolytes. The corresponding integrated charge plots for divalent salts corroborate two main features of the surface charge amplification previously detected in Figure 5, namely that, for charged colloids in the presence of small coions (1) the surface charge amplification always exists, and (2) that the maximum value of the surface charge amplification is limited to occur at the outer Helmholtz plane. In all the systems displayed in Figure 6, the magnitude of the cumulative charge is notably accentuated. As a result, significant surface charge amplification is observed in comparison with the $+1:-1$ cases. As an example, note that, for $\sigma_0 = 0.01\text{ C/m}^2$, $Q(r' = 1 + \gamma_b)$ has the values $2.260e$, $3.422e$ and $3.932e$ for Figure 6(a)–(c) in the upper row, respectively, whereas the values $17.355e$,

23.892e and 25.171e are observed for $Q(r' = 1 + \gamma_b)$ in Figure 6(d)–(f) in the lower row, respectively.

The various above-mentioned features of the surface charge amplification can be also explained in terms of the behaviour of the ionic profiles, $g_s(r')$ and $g_b(r')$. In particular, Equation (15) is specially relevant for the surface charge amplification since it relates the first derivative of the integrated charge with the total local charge, $\rho_c(r')$, which in our case is proportional to the difference between the ionic profiles, i.e., $\rho_c(r') = \rho_s z_s e (g_s(r') - g_b(r'))$. As an example of the generic comportment of the radial distribution functions for all the cases presented in Figures 5 and 6, wherein coions are smaller than counterions, in Figure 7, graphs of two representative systems are included. There, we can appreciate that the functions $g_s(r')$ and $g_b(r')$ approach monotonically to their bulk value and, accordingly, we realise that $\rho_c(r')$ is a piecewise one-signed function, whose magnitude is never zero, namely, for $1 + \gamma_s \leq r' < 1 + \gamma_b$, since $g_b(r') = 0$, we have $Q_0 \rho_c(r') \geq 0$ and, thus, $Q_0 (dQ(r')/dr') \geq 0$, whereas, for $1 + \gamma_b \leq r' < \infty$, and due to the electroneutrality condition, $Q_0 \rho_c(r') \leq 0$ and, thus, $Q_0 (dQ(r')/dr') \leq 0$. Therefore, from Figure 7, we conclude that, in the URMGC theory, for a system with coions smaller than counterions, the first derivative of $Q(r')$ is discontinuous at $r' = 1 + \gamma_b$, and that, at the same spatial point, $Q(r')$ has its unique extremum (a cusp). In other words, we have found that, in a mean-field description of size-asymmetric semi-punctual-ions systems with small coions, the growth of the magnitude of $Q(r')$ and the maximum intensity of the associated charge amplification phenomenon are always localised inside the Helmholtz region ($1 + \gamma_s \leq r' \leq 1 + \gamma_b$), analogously to the localisation observed for the sign change of $Q(r')$ (or the onset of charge reversal) and its associated extremum in electric double layers with small counterions. In addition, it is noticeable that, this time differently from charge reversal with small counterions, the effect of the surface charge amplification in the URMGC theory does not require the oscillation of the radial distribution functions and the mean electrostatic potential to occur.

3.2. Size- and charge-asymmetric electrolytes

In the past, URMGC studies of charge reversal and surface charge amplification have been focused on systems with symmetrical valences [17–19,28,38]. As a novelty, in the next paragraphs, we review some URMGC results for spherical electric double layers with fully size- and charge-asymmetric semi-punctual cations and anions.

In Figure 8(a)–(d), we portray the integrated charge of a macroion immersed in $-1: +2$, $-1: +3$, $-2: +1$ and $-3: +1$ electrolytes, respectively. In all those instances, the radius of the macroion is $R = 10 \text{ \AA}$, but the colloidal surface charge density σ_0 is varied. The concentration of the smallest ionic species and the ionic size-asymmetry of all electrolytes are fixed to the following values: $\rho_s = 0.5 M$, r_s

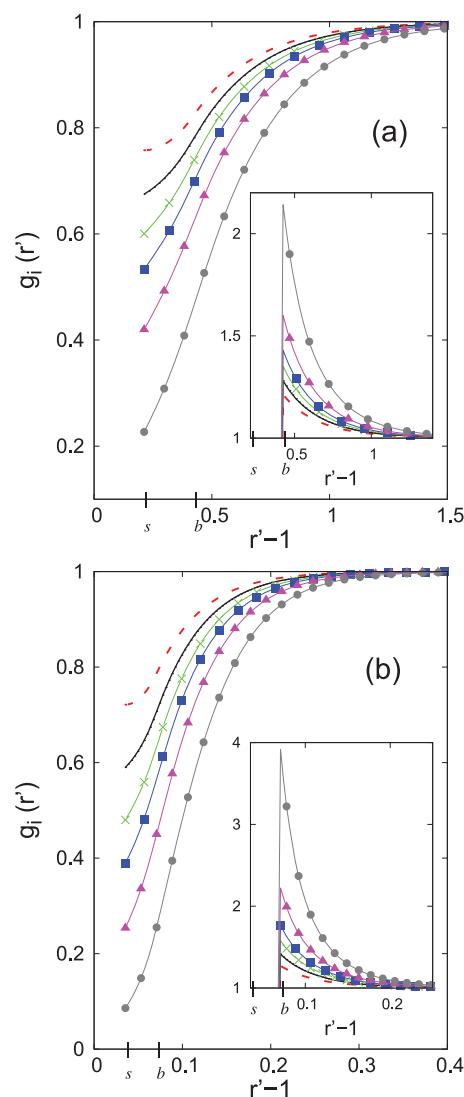


Figure 7 Radial distribution functions of monovalent and divalent size-asymmetric $z: z$ ions around a macroion for different surface charge densities. In panel (a), the macroion has a radius $R = 10 \text{ \AA}$ and it is immersed in a $+1: -1$, 1 M electrolyte with ionic ‘radii’ $r_s = 2.125 \text{ \AA}$ and $r_b = 4.25 \text{ \AA}$. In panel (b), the macroion has a radius $R = 30 \text{ \AA}$ and it is immersed in a $+2: -2$, 1 M electrolyte with ionic ‘radii’ $r_s = 1.0625 \text{ \AA}$ and $r_b = 2.125 \text{ \AA}$. The correspondence between lines and surface charge densities is the same as that used in Figure 2.

$= 2.125 \text{ \AA}$ and $r_b = 4.25 \text{ \AA}$. Given that in all these graphs the counterions are the smallest ionic species, we can observe charge reversal in the integrated charge curves. Figure 8(a) and 8(b), in the upper row, shows the effect on charge reversal due to the variation of the characteristics (i.e., valence and concentration) of the biggest ionic species (coions), whereas Figure 8(c) and 8(d), in the lower row, illustrates the sequels of changing the valence of the smallest ion type (counterions). Clearly, there is a minor enhancement of the charge reversal when we contrast the $-1: +2$ and $-1: +3$ systems of Figure 8(a) and 8(b) than the increment found after comparing the $-2: +1$ and $-3: +1$ cases of

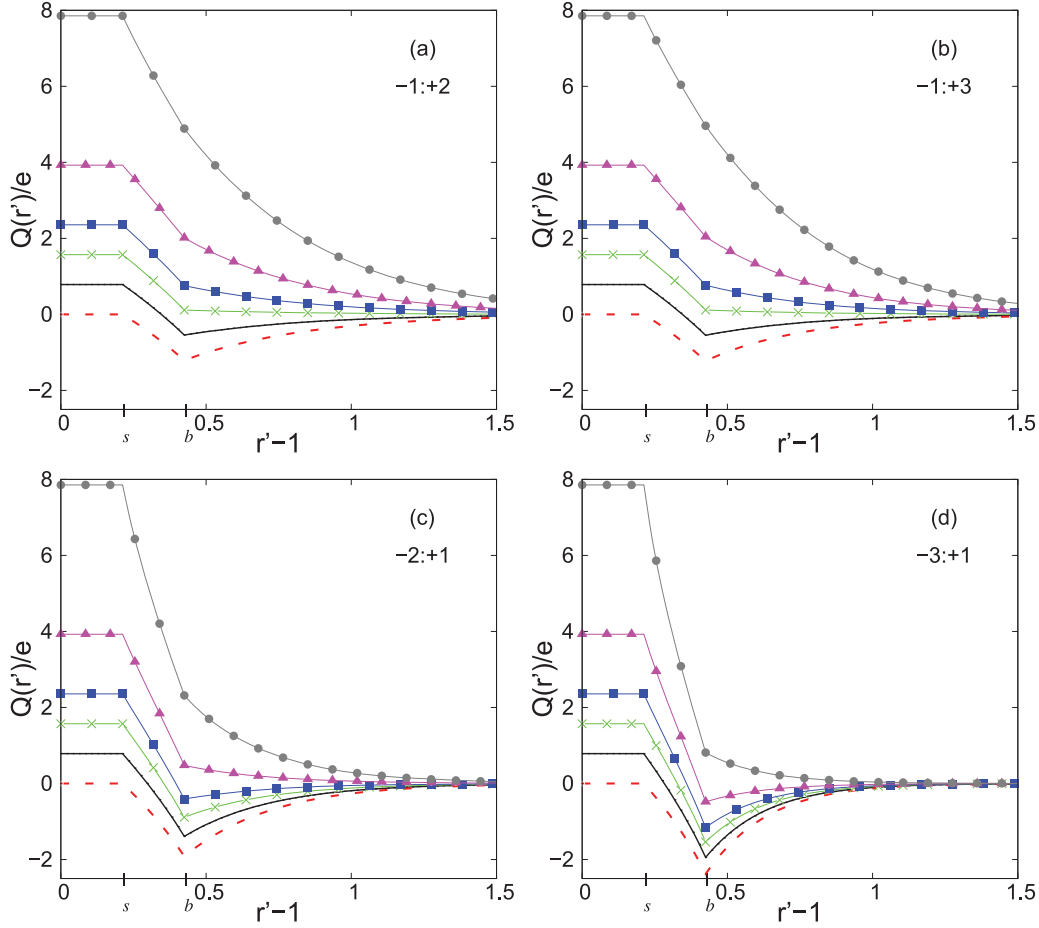


Figure 8 Integrated charge, $Q(r')$, around a macroion as a function of the distance to its surface. The charged colloid has a radius $R = 10 \text{ \AA}$ and it is immersed in different size- and charge-asymmetric electrolytes for a fixed $\rho_s = 0.5 \text{ M}$ of the small counterions. The ionic ‘radii’ are $r_s = 2.125 \text{ \AA}$ and $r_b = 4.25 \text{ \AA}$. The correspondence between lines and surface charge densities is the same as that used in Figure 2.

Figure 8(c) and 8(d) (e.g., for $\sigma = 0.01 \text{ C/m}^2$, the minimum value of $Q(r')$, occurred at $r' = 1 + \gamma_b$, is $-0.543e$ for a $-1: +2$ salt and $-0.550e$ for a $-1: +3$ one, in the upper row, in contrast with $-1.392e$ for a $-2: +1$ electrolyte and $-1.943e$ for a $-3: +1$ one, in the lower row). To understand this fact, let us consider the following arguments. A quick examination of Equations (9)–(11) evidences that the ionic radial distribution functions have a functional dependence on the distance r' and on the parameters A , B , γ_s , γ_b and λ , i.e., $g_{s,b}(r'; A, B, \gamma_s, \gamma_b, \lambda)$. Additionally, from Equation (13), $Q(r')/e$ can be rewritten as

$$\frac{Q(r')}{e} = \begin{cases} z_M \left[1 + \left(\frac{B}{A} \right) \int_{1+\gamma_s}^{r'} g_s(t') t'^2 dt' \right], & \text{for } 1 + \gamma_s \leq r' < 1 + \gamma_b, \\ z_M \left[1 + \left(\frac{B}{A} \right) \int_{1+\gamma_s}^{1+\gamma_b} g_s(t') t'^2 dt + \int_{1+\gamma_b}^{r'} (g_s(t') - [g_s(t')]^\lambda) t'^2 dt' \right], & \text{for } 1 + \gamma_b \leq r' < \infty, \end{cases} \quad (18)$$

with $z_M = Q_0/e = 4\pi R^2 \sigma_0/e$. Notice that, in the cases presented in Figure 8(a) and 8(b), the valence and concentration of the smallest species are kept constant ($z_s = -1$ and $\rho_s = 0.5 \text{ M}$, respectively). Thus, for a given macroparticle charge and according to Equation (18), the possible changes in the $Q(r')/e$ graphs will be originated solely by the variation of the parameter $\lambda = z_b/z_s$ (which goes from -2 to -3 in the upper row panels, due to change of z_b from $+2$ to $+3$). Hence, this weak dependence of the integrated charge on λ allows us to foresee that the change in the integrated charge curves, when the valence and concentration of the big coions are modified, will be slight. Such a prediction can be confirmed by looking, for example, the $Q(r')/e$ profiles for $\sigma = 0.01 \text{ C/m}^2$ in Figure 8(a) and 8(b). On the other hand, notice that a minimum variation in the valence of the smallest ionic species, at a fixed concentration $\rho_s = 0.5 \text{ M}$, yields a significant variation in the corresponding A , B and λ parameters (see, e.g., the $-2: +1$ and $-3: +1$ systems in Figure 8(c) and 8(d)). As a consequence, we should expect

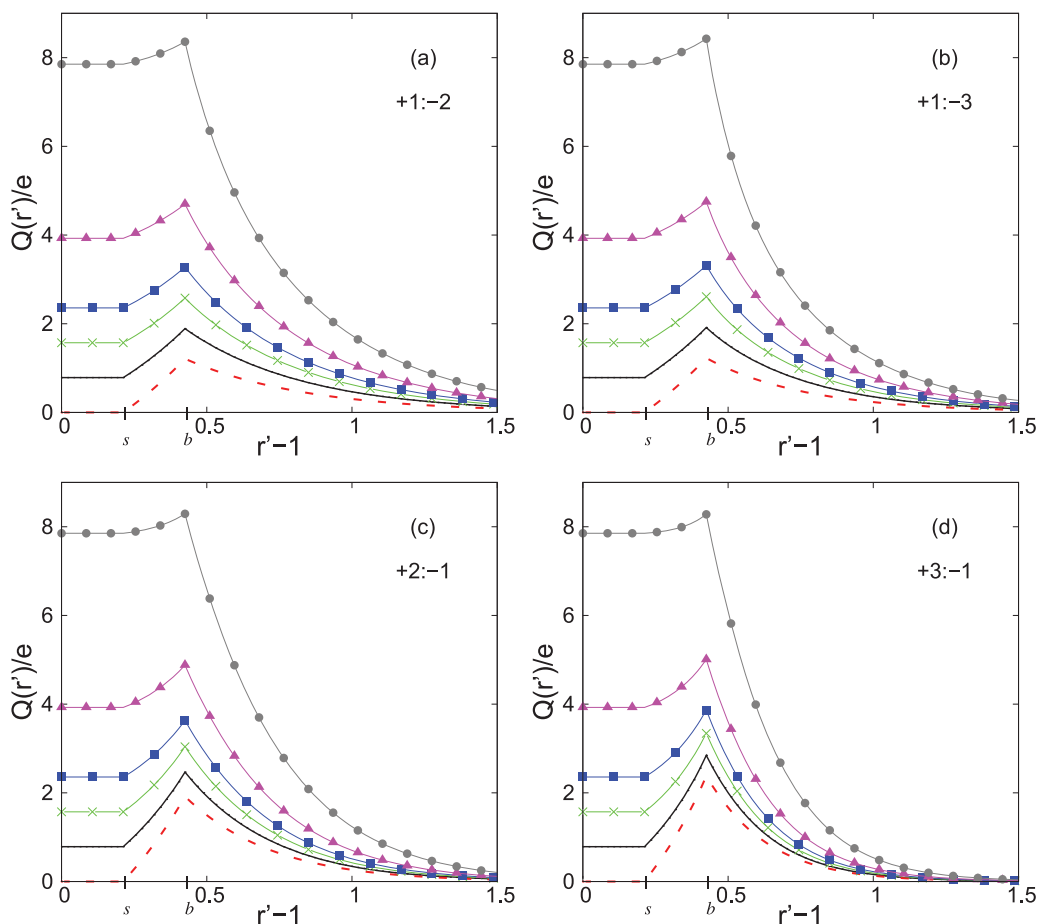


Figure 9 Integrated charge, $Q(r')$, around a macroion as a function of the distance to its surface. The charged colloid has a radius $R = 10 \text{ \AA}$ and it is immersed in different size- and charge-asymmetric electrolytes for a fixed $\rho_s = 0.5 \text{ M}$ of the small coions. The ionic ‘radii’ are $r_s = 2.125 \text{ \AA}$ and $r_b = 4.25 \text{ \AA}$. The correspondence between lines and surface charge densities is the same as that used in Figure 2.

a more significant contrast between the corresponding $Q(r')/e$ plots for a given surface charge density σ_0 , as it is displayed in Figure 8(c) and 8(d). Such a rationale anticipates and explains the discernible enhancement of the charge reversal effect occurring when the valence of the small counterions is increased from -2 to -3 at the same ρ_s concentration (see, for instance, the $\sigma = 0.01 \text{ C/m}^2$ curves). Therefore, a whole consideration of Figure 8(a)–(d) evinces the fact that altering the valence of the small counterions, at a fixed ρ_s concentration, implies larger effects on charge reversal than changing the properties of the big coions, i.e., for not very high colloidal charges, the *small* counterions dominate the electric double layer.

In Figure 9, integrated charge data for size- and charge-asymmetric systems display the occurrence of surface charge amplification due to the presence of coions smaller than counterions. Figure 9(a)–(d) portrays the integrated charge for a macroion of radius $R = 10 \text{ \AA}$ at different surface charge densities. This macroion is immersed in electrolytic ambients of valences $+1:-2$, $+1:-3$, $+2:-1$ and $+3:-1$ corresponding to Figure 9(a)–(d), respectively. In

all these instances, the concentration of small ions and the ionic closest approach distances to the macroion have the constant values $\rho_s = 0.5 \text{ M}$, $r_s = 2.125 \text{ \AA}$ and $r_b = 4.25 \text{ \AA}$, respectively.

Panels 9(a) and 9(b), in the upper row, show that the exclusive modification of the big counterions attributes (valence and concentration) provokes a little increment in the surface charge amplification (e.g., for $\sigma = 0.01 \text{ C/m}^2$, the maximum $Q(r' = 1 + \gamma_b)$ is $1.890e$ for a $+1:-2$ salt and $1.913e$ for a $+1:-3$ one). Meanwhile, panels 9(c) and 9(d) in the lower row exhibit cases for which the valence of the small coions is variated. In these last figures, when z_s passes from $+2$ to $+3$, $Q(r')/e$ changes more notably (for instance, for $\sigma = 0.01 \text{ C/m}^2$, the maximum $Q(r' = 1 + \gamma_b)$ is $2.466e$ for a $+2:-1$ electrolyte and $2.845e$ for a $+3:-1$ one). Once more, the trends observed in Figure 9 can be rationalised recurring to the same ideas based on Equation (18), and priorly used for Figure 8. In these terms, notice that, from the fundamental parameters A , B , γ_s , γ_b and λ , only the last one variates in Figure 9(a) and 9(b). This anticipates minor changes in the $Q(r')/e$ curves and in

the surface charge amplification effect. Complementarily, in the case of Figure 9(c) and 9(d), altering the valence of the small coions affects significantly the parameters A , B and λ , which accounts for the major differences in the corresponding integrated charges and the more pronounced surface charge amplification when z_s increases. Thence, from the contrast between the $Q(r')/e$ plots in the upper and lower rows of Figure 9, we learn that, at a fixed concentration of the smallest ionic species, a modification of the valence of the small coions impacts largely the augmentation of the net charge enclosed by the outer Helmholtz plane or, alternatively, that, for low and medium surface charge densities of the bare macroion σ_0 , a major change of the *small* multivalent coions increases significantly the colloidal surface charge amplification.

Summarising the findings derived from the charge-asymmetric cases of Figures 8 and 9, we then arrive to the following conclusion: let us consider a binary size-asymmetric semi-punctual electrolyte surrounding a weakly/moderate charged spherical colloid. Hence, if the concentration of the smallest species is fixed, a change in the valence of the smallest ions affects in a more important manner the phenomena of charge reversal and surface charge amplification in comparison to a change in the valence of the biggest ions, independently of the colloidal polarity. In other words, at low/medium colloidal surface charges and a fixed concentration of the smallest ionic species, the phenomena of charge reversal and surface charge amplification are affected more significantly by a change on the valence of the smallest ionic species, independently if they are coions or counterions, i.e., under the previous conditions, small ions mainly rule or determine the structural and thermodynamic properties of fully asymmetric semi-punctual electrolytes described by the URMGC theory.

4. Conclusions

In this work, we have provided a theoretical mean-field description of a fully size- and charge-asymmetric semi-punctual binary electrolyte surrounding a charged spherical colloid. The proposed integral equations formulation, corresponding to the URMGC theory, has been used to study microscopic ionic properties of the electric double layer, such as the ionic profiles and the integrated charge. The corresponding integral equations were recast in a normalised (or a dimensional) form. Even though there exist diverse possibilities to define the fundamental non-dimensional theoretical parameters, the current choice has allowed us to write other structural electric double layer properties (e.g., the integrated charge or the mean electrostatic potential) in terms of the same set of non-dimensional parameters. The investigation of these structural properties has allowed us to observe the phenomena of charge reversal and surface charge amplification in the regime of

low/moderate colloidal charges. We have demonstrated that (1) the appearance of charge reversal is directly related to the existence of extrema in the mean electrostatic potential and ionic profile of the smallest ionic species; (2) the raise and the extremum of the surface charge amplification are due to the fact that the local ionic charge density is a piecewise one-signed function; (3) in the presence of charge reversal, there is only one change of sign of the associated integrated charge (indicating the corresponding onset) that is always *localised* inside the Helmholtz zone; and (4) that the possible extrema of the charge reversal and surface charge amplification are unique and are *localised* precisely at the outer Helmholtz plane. As the charge reversal and surface charge amplification are not restricted to appear necessarily inside the Helmholtz zone, the *localisation* effect advanced in (3) and (4) is enticing because it offers a prescription to discriminate the origin of these phenomena in more sophisticated theories that go beyond our semi-punctual URMGC approach.

On the other hand, as already mentioned in Section 2, in their pioneering URMGC paper of 1982 [32], Valleau and Torrie established the well-known dominance of the counterions, i.e., that, in the limit of very large surface charges, ‘... we expect the double layer properties of a dilute (fully asymmetric) electrolyte to become similar to those of a completely asymmetric electrolyte having an effective size equal to that of the counterion...’. In other words, according to this principle, the counterions define essentially the comportment of highly charged electric double layers. The relevance of this counterion predominance for double layer studies cannot be overlooked when we note that, even if this remark is strictly valid at the Poisson–Boltzmann level, its ‘obviousness’ has converted it in a wonted assumption that has been frequently applied in an improper manner in many theoretical and simulational electric double layer analysis that go beyond the classical Poisson–Boltzmann equation [42,46–53]. Notably, this inappropriate usage of the original statement of Valleau and Torrie for the URMGC theory has been plainly evidenced and amended in a couple of papers concerning the spherical electric double layer of primitive model electrolytes by Guerrero-García and collaborators [17,38]. In this context, the present semi-punctual mean-field investigation of charge reversal and surface charge amplification in size- and charge-asymmetric systems acquires a particular significance, since it reveals a principle that nicely complements the standard predominance of counterions at high surface charges introduced by Valleau and Torrie, this time in the opposite surface charge regime. Specifically, we have shown that, according to the URMGC theory, a change in the valence of the smallest ionic species, independently if they are coions or counterions, has a higher impact in the electric double layer than a change in the valence of the biggest ionic species if the concentration of the smallest ions is fixed and the colloidal surface charge is low/moderate. That is, the

structural and thermodynamic properties of a fully size- and charge-asymmetric semi-punctual binary electrolyte surrounding a weakly/moderately charged colloid are dominated by changes in the valence of small ions regardless of the colloidal polarity if they are present at a fixed concentration. The dominance of small ions has been illustrated here by showing the significant impact that the specific characteristics of the smallest ionic species yield in the corresponding charge reversal and surface charge amplification phenomena, even in a simple semi-punctual ions mean-field approach.

Finally, even if the conclusions obtained in this communication, e.g., the dominance of small ions at very low colloidal charges, are strictly valid for semi-punctual electric double layer systems only at the URMGC level, it remains to be determined if such findings are still applicable in more accurate descriptions of the electric double layer, for instance, in the primitive model of an electrolyte. Work in this direction is currently in progress.

Acknowledgements

Fruitful discussions with Dr. Martín Chávez-Páez and the computer assistance from the technicians at the IF-UASLP are gratefully acknowledged.

Disclosure statement

No potential conflict of interest was reported by the authors.

Funding

Evelyn Angélica Barrios-Contreras and Enrique González-Tovar wish to thank PROMEP and the Mexican National Council of Science and Technology (CONACYT) for their financial support. Guillermo Iván Guerrero-García acknowledges CONACYT for the financial funding via the program ‘Cátedras CONACYT para Jóvenes Investigadores’.

ORCID

Guillermo Iván Guerrero-García  <http://orcid.org/0000-0002-3174-2643>

References

- [1] W.B. Russel, D.A. Saville and W.R. Schowalter, *Colloidal Dispersions* (Cambridge University Press, Cambridge, 1992).
- [2] R.J. Hunter, *Foundations of Colloid Science* (Oxford University Press, Oxford, 2001).
- [3] R.D. Cadena-Nava, M. Comas-García, R.F. Garmann, A.L.N. Rao, C.M. Knobler, and W.M. Gelbart, *J. Virol.* **86**, 3318 (2012).
- [4] A. Moncho-Jordá, J.A. Anta, and J. Callejas-Fernández, *J. Chem. Phys.* **138**, 134902 (2013).
- [5] A. Moncho-Jordá, *J. Chem. Phys.* **139**, 064906 (2013).
- [6] C.N. Patra, *J. Chem. Phys.* **141**, 104503 (2014).
- [7] C.N. Patra, *J. Chem. Phys.* **141**, 184702 (2014).
- [8] Z. Ovanesyan, B. Medasani, M.O. Fenley, G.I. Guerrero-García, M. Olvera de la Cruz, and M. Marucho, *J. Chem. Phys.* **141**, 225103 (2014).
- [9] G.I. Guerrero-García and M. Olvera de la Cruz, *J. Chem. Theory Comput.* **9**, 1 (2012).
- [10] G.I. Guerrero-García, Y. Jing, and M. Olvera de la Cruz, *Soft Matter* **9**, 6046 (2013).
- [11] P. González-Mozuelos, G.I. Guerrero-García, and M. Olvera de la Cruz, *J. Chem. Phys.* **139**, 064709 (2013).
- [12] G.I. Guerrero-García, P. González-Mozuelos, and M. Olvera de la Cruz, *ACS Nano* **7**, 9714 (2013).
- [13] G.I. Guerrero-García and M. Olvera de la Cruz, *J. Phys. Chem. B* **118**, 8854 (2014).
- [14] E. Gonzales-Tovar, M. Lozada-Cassou, and D. Henderson, *J. Chem. Phys.* **83**, 361 (1985).
- [15] F. Jiménez-Ángeles and M. Lozada-Cassou, *J. Phys. Chem. B* **108**, 7286 (2004).
- [16] J. Lyklema, *Colloids Surf. A* **291**, 3 (2006).
- [17] G.I. Guerrero-García, E. González-Tovar, and M. Chávez-Páez, *Phys. Rev. E* **80**, 021501 (2009).
- [18] G.I. Guerrero-García, E. González-Tovar, M. Chávez-Páez, and M. Lozada-Cassou, *J. Chem. Phys.* **132**, 054903 (2010).
- [19] G.I. Guerrero-García, E. González-Tovar, and M. Olvera de la Cruz, *Soft Matter* **6**, 2056 (2010).
- [20] A. Naji, M. Ghodrat, H. Komaie-Moghaddam, and R. Podgornik, *J. Chem. Phys.* **141**, 174704 (2014).
- [21] G.I. Guerrero-García, E. González-Tovar, and M. Olvera de la Cruz, *J. Chem. Phys.* **135**, 054701 (2011).
- [22] J. Lyklema, *J. Colloid Interface Sci.* **392**, 102 (2013).
- [23] W.M. Gelbart, R.F. Bruinsma, P.A. Pincus, and V.A. Parsegian, *Phys. Today* **53**, 38 (September, 2000).
- [24] E. García-Giménez, A. Alcaraz, and V.M. Aguilera, *Phys. Rev. E* **81**, 021912 (2010).
- [25] A. Kubickova, T. Krizek, P. Coufal, M. Vazdar, E. Wernersson, J. Heyda, and P. Jungwirth, *Phys. Rev. Lett.* **108**, 186101 (2012).
- [26] Y. He, D. Gillespie, D. Boda, I. Vlassiuk, R.S. Eisenberg, and Z.S. Siwy, *J. Am. Chem. Soc.* **131**, 5194 (2009).
- [27] J. Hoffmann and D. Gillespie, *Langmuir* **29**, 1303 (2013).
- [28] J. Yu, G.E. Aguilar-Pineda, A. Antillón, S.-H. Dong, and M. Lozada-Cassou, *J. Colloid Interface Sci.* **295**, 124 (2006).
- [29] M. Gillan, B. Larsen, M.P. Tosi, and N.H. March, *J. Phys. C* **9**, 889 (1976).
- [30] L.B. Bhuiyan and C.W. Outhwaite, *J. Chem. Phys.* **116**, 2650 (2002).
- [31] L.B. Bhuiyan and C.W. Outhwaite, *Physica A* **339**, 199 (2004).
- [32] J.P. Valleau and G.M. Torrie, *J. Chem. Phys.* **76**, 4623 (1982).
- [33] E. González-Tovar and M. Lozada-Cassou, *J. Phys. Chem.* **93**, 3761 (1989).
- [34] L.B. Bhuiyan, L. Blum, and D. Henderson, *J. Chem. Phys.* **78**, 442 (1983).
- [35] R.B. McBroom and D. McQuarrie, *Cell Biophys.* **11**, 65 (1987).
- [36] M.M. Huerta, J.E. Curry, and D.A. McQuarrie, *Clays Clay Miner.* **40**, 491 (1992).
- [37] M. Lozada-Cassou, R. Saavedra-Barrera, and D. Henderson, *J. Chem. Phys.* **77**, 5150 (1982).
- [38] G.I. Guerrero-García, E. González-Tovar, M. Lozada-Cassou, and F.J. Guevara-Rodríguez, *J. Chem. Phys.* **123**, 034703 (2005).
- [39] M. Quesada-Pérez, E. González-Tovar, A. Martín-Molina, M. Lozada-Cassou, and R. Hidalgo-Álvarez, *Chem. Phys. Chem.* **4**, 234 (2003).

- [40] K. Wang, Y.X. Yu, and G.H. Gao, *Phys. Rev. E* **70**, 011912 (2004).
- [41] S. Iyanaga and Y. Kawada, editors, *Encyclopedic Dictionary of Mathematics* (MIT Press, Cambridge, MA, 1977), Vol. I, Article 218 (X.10).
- [42] Y.X. Yu, J.Z. Wu, and G.H. Gao, *J. Chem. Phys.* **120**, 7223 (2004).
- [43] L.B. Bhuiyan and C.W. Outhwaite, *Condens. Matter Phys.* **8**, 287 (2005).
- [44] E.-Y. Kim and S.-C. Kim, *J. Chem. Phys.* **140**, 154703 (2014).
- [45] E.-Y. Kim, S.-C. Kim, Y.-S. Han, and B.-S. Seong, *Mol. Phys.* (2014). DOI:10.1080/00268976.2014.985753.
- [46] G.M. Torrie and J.P. Valleau, *J. Phys. Chem.* **86**, 3251 (1982).
- [47] S.L. Carnie and G.M. Torrie, *Adv. Chem. Phys.* **56**, 141 (1984).
- [48] U.M.B. Marconi, J. Wiechen, and F. Forstmann, *Chem. Phys. Lett.* **107**, 609 (1984).
- [49] A.F. Khater, D. Henderson, L. Blum, and L.B. Bhuiyan, *J. Phys. Chem.* **88**, 3682 (1984).
- [50] D. Boda, D.H.W.R. Fawcett, and S. Sokolowski, *J. Chem. Phys.* **116**, 7170 (2002).
- [51] L. Bari Bhuiyan and C.W. Outhwaite, *Phys. Chem. Chem. Phys.* **6**, 3467 (2004).
- [52] M. Valiskó, D. Henderson, and D. Boda, *J. Phys. Chem. B* **108**, 16548 (2004).
- [53] V. Dorvilien, C.N. Patra, L.B. Bhuiyan, and C.W. Outhwaite, *Condens. Matter Phys.* **16**, 43801 (2013).